Energy 333 (2025) 137416

Contents lists available at ScienceDirect

Energy

journal homepage: www.elsevier.com/locate/energy

Parametric study of a thermoelectric-based battery thermal management system with vapor chambers for high discharge rate

Ding Luo [a,b], Zihao Wu [a], Haifeng Wu [a], Hao Chen [a,*], Peng Zhang [a], Bingyang Cao [b,**]

[a] Shaanxi Key Laboratory of New Transportation Energy and Automotive Energy Saving, School of Energy and Electrical Engineering, Chang'an University, Xi'an, China
[b] Key Laboratory for Thermal Science and Power Engineering of Ministry of Education, Department of Engineering Mechanics, Tsinghua University, Beijing, 100084, China

ARTICLE INFO

Handling editor: X Ou

Keywords:
Thermoelectric cooler
Battery thermal management system
Vapor chamber
High discharge rate
Maximum temperature

ABSTRACT

This work introduces a battery thermal management system (BTMS) which combines thermoelectric coolers (TECs) and vapor chambers (VCs) to realize effective temperature regulation for batteries operating under high discharge rates. Additionally, a thermal-electric coupling model is developed to study the influence of various parameters on the system's thermal performance, including TEC input current, thermoelectric leg height, and air cooling coefficient. It is revealed that while TECs with shorter leg heights yield higher coefficient of performance (COP) and cooling power, they are limited by their capacity to withstand lower temperature differences. With the elevation of TEC input current, the maximum temperature of batteries first drops and then augments, while the variation trend for the temperature difference remains opposite. Through detailed analysis, the optimal operating conditions are determined to be an input current of 3 A, a leg height of 1.4 mm, and an air cooling coefficient of 50 W/(m^2·K). Under these conditions, the BTMS achieves a maximum battery temperature of 300.94 K and a temperature difference of 4.78 K. In comparison to a BTMS without TECs, the use of TECs reduces the maximum battery temperature by 13.58 K, with only a slight increase of 0.29 K in temperature difference. This research offers a fresh perspective on the practical application of TECs in thermal management systems, highlighting their potential for enhancing battery performance under demanding conditions.

Nomenclature

Symbols

C	specific heat, J/(kg·K)
$\vec{E}$	electric field density vector, V/m^2
h	heat transfer coefficient, W/(m^2·K)
H	height, mm
I	current, A
$\vec{J}$	current density vector, A/m^2
k	thermal conductivity, W/(m·K)
P	power, W
Q	heat or volumetric heat, W or W/m^3
R	resistance, Ω
T	temperature, K
V	volume, m^3
σ	electrical conductivity, S/m

Subscripts

b	battery
c	cold side
co	copper electrodes
h	hot side
in	input
m	material
n	n-type legs
p	p-type legs

Abbreviations

BTMS	battery thermal management system
COP	coefficient of performance
HP	heat pipe
LFP	lithium iron phosphate
LIB	lithium-ion battery
PCM	phase change material
TEC	thermoelectric cooler
VC	vapor chamber

Greek symbols

α	seebeck coefficient, μV/K
λ	thermal conduction, W/K
ϕ	electrical potential, V

(continued on next column)

(continued)

1. Introduction

The wide adoption of new energy vehicles holds crucial significance in alleviating the energy crisis and environmental degradation resulting from the extensive use of traditional fuels [1]. Serving as the primary energy storage unit for new energy vehicles, lithium-ion batteries (LIBs) exhibit notable advantages, including high energy density, efficiency, and extended cycle life [2–4]. Nevertheless, LIBs emit a substantial amount of heat during their operation, and insufficient heat dissipation may result in heat accumulation within the battery pack, potentially

* Corresponding author.
** Corresponding author.
E-mail addresses: chenhao@chd.edu.cn (H. Chen), caoby@tsinghua.edu.cn (B. Cao).

https://doi.org/10.1016/j.energy.2025.137416
Received 10 April 2025; Received in revised form 14 June 2025; Accepted 4 July 2025
Available online 11 July 2025

compromising the battery lifespan, or even causing explosions [5]. As illustrated in Fig. 1, the charging performance of the LIB remains nearly unaffected within the temperature range of 293.15 K–313.15 K [6,7]. However, when the temperature falls below 293.15 K, both the charging and discharging capabilities of the cell experience a significant decline. This degradation is primarily due to the sharp increase in internal resistance at low temperatures, which severely limits the charge/discharge capacity of the LIB [8]. Furthermore, thermal uniformity—defined as the consistency of temperature distribution among individual batteries within a battery pack—is also a key factor influencing the performance of LIBs [9]. Non-uniform temperature distributions can lead to imbalanced electrochemical reactions, accelerated aging, and reduced overall system efficiency [10]. It has been reported that the maximum temperature difference within a battery pack should be limited to below 5 K to ensure balanced performance and minimize degradation risks [11,12]. Consequently, a favorable battery thermal management system (BTMS) is crucial to ensure that the operating temperature of LIBs within an efficient range, which not only prolongs battery cycle life but also mitigates the risk of thermal runaway [13].

Air-based BTMS, phase change material (PCM)-based BTMS, liquid-based BTMS, and heat pipe (HP)-based BTMS are four major categories within the mainstream BTMS [14]. The advantages, disadvantages, limitations, and typical thermal conductivity ranges of four representative BTMS are summarized in Table 1 [15–17]. Generally, air cooling remains the preferred cooling technology because of its low price and simple structure. However, the low thermal conductivity and specific heat of air cooling restrict its heat dissipation efficiency [18]. Therefore, enhancing the heat transfer of the air-based BTMS is an important focus for future research in this system [19]. In comparison of air cooling method, liquid-based BTMS offers superior heat transfer performance [20]. However, liquid cooling also has drawbacks, including a more complex structure, increased system weight, risk of leakage, and poor temperature uniformity [21]. Unlike the aforementioned two active cooling methods, the PCM-based cooling method is a passive one that utilizes the latent heat of PCMs to dissipate the heat generated by battery cells [22]. This reduces energy consumption and ensures uniform thermal distribution. Nevertheless, the low thermal conductivity of PCMs significantly impacts cooling efficiency and limits their widespread commercial use [23]. In addition, as an auxiliary system, the BTMS must not only meet the fundamental requirements of thermal management but also exhibit superior safety, rapid response, lightweight design, compact structure, and ease of maintenance [24].

On the basis of the liquid-gas phase transition, HPs exhibit characteristics of small volume and lightweight, which can be manufactured in various shapes based on available space and have no maintenance cost [25]. Besides, HPs possess an exceptionally high thermal conductivity, marking them as a promising cooling method. Tran et al. [26] performed a comparative study of the thermal performance of a flat plate HP cooling system and a traditional radiator under different positions and conditions; Their findings demonstrated that incorporating HPs can lower the thermal resistance of a conventional heat sink by 20 % under low airflow cooling and by 30 % under natural convection, and it is not feasible to maintain the temperature of batteries below 323.15 K solely through the use of radiators. Jouhara et al. [27] developed a BTMS based on flat HPs to improve temperature uniformity during high discharge rate operation and studied its performance using an experimentally verified model; Simulations indicated that the utilization of flat HPs not only effectively lowers the peak temperature and temperature difference but also minimizes the associated energy consumption. In contrast to liquid cooling and air cooling techniques, the HP-based one improved the heat dissipation and thermal uniformity of batteries. Ye et al. [28] developed a composite BTMS integrated with HPs and proposed various air-cooling strategies; They reported that the integration of HP cooling and air cooling is infeasible for managing battery temperature at a high discharge rate, primarily because of the performance limitation of air cooling on the condensation side of HPs. The literature indicates that HPs, with their high thermal conductivity, are effective in reducing battery temperature and improving temperature uniformity. Moreover, the passive cooling nature of HPs helps lower energy costs. However, the selection of active cooling methods for the condensation side of the HP significantly influences its overall performance.

Thermoelectric refrigeration, as a novel cooling approach, has attracted significant attention in recent years. As a solid-state system, thermoelectric cooling offers rapid response, precise temperature control, and no refrigerant pollution [29]. With the rapid advancement of thermoelectric technology, an increasing number of thermoelectric devices are being integrated into various applications, including refrigerators [30], air conditioners [31], and battery thermal management [32]. TECs can achieve near-instantaneous response times (milliseconds to seconds) due to the absence of moving parts [33], outperforming passive systems such as PCMs, which rely on relatively slow phase change processes, as well as liquid cooling systems, whose response times are constrained by pump startup delays and fluid flow inertia—typically ranging from several seconds to tens of seconds. Compared to passive thermal management components such as PCM and VCs, which dissipate heat without external energy input, TECs typically exhibit a relatively low coefficient of performance (COP), usually around 0.5. Integrating TECs with highly conductive passive elements like VCs helps mitigate this efficiency limitation by enhancing overall system-level thermal performance. Moreover, unlike traditional cooling methods, TECs uniquely offer the capability to provide both cooling and heating by adjusting their input current, a distinct advantage that is particularly beneficial for LIBs operating under varying environmental conditions in electric vehicles. Suh et al. [34] employed thermoelectric coolers (TECs) in a BTMS, demonstrating the feasibility of such devices through experiments and simulations; They found that TECs can realize the thermal dissipation of the BTMS with a relatively small input of electrical energy, and the rapid response of TECs enhances

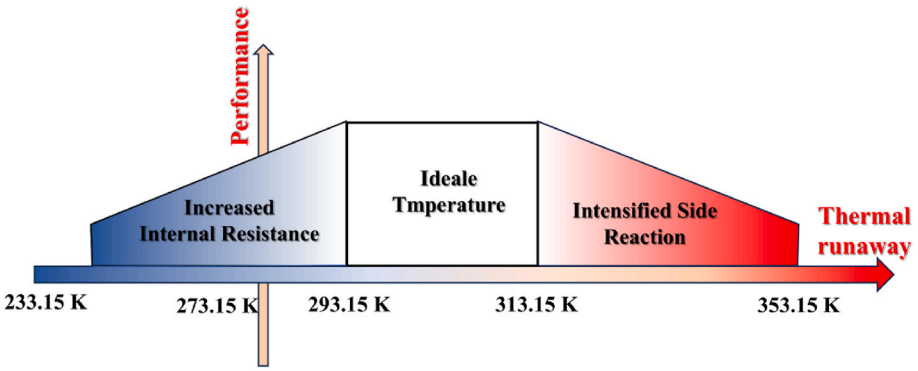

Fig. 1. Effect of battery temperature on performance.

Table 1
Comparison of common BTMS methods with respect to thermal efficiency, complexity, safety, and thermal conductivity [15–17].

BTMS Method	Thermal Efficiency	System Complexity	Safety	Thermal Conductivity Range (W/m·K)	Advantages	Disadvantages
Air Cooling	Low	Low	High	~0.025	Simple design, low cost, safe	Limited cooling capacity, poor thermal uniformity
Liquid Cooling	High	High	Medium	~0.6 (water) – 2.0 (coolants)	High heat removal rate, stable cooling	Complex design, potential leakage risk
PCM	Medium	Medium	High	~0.2–0.5	Passive operation, improved thermal uniformity	Limited cooling duration, needs regeneration
HP	High	Medium	High	Effective thermal conductivity up to 10,000+	High thermal conductivity, passive operation	Limited by saturation and orientation constraints, no active cooling

the thermal performance of batteries. Song et al. [35] disclosed a BTMS incorporating TECs and PCMs and performed a simulation analysis on the thermal performance at various charge-discharge rates; Their findings indicated that the battery temperature could reach the required standards, regardless of whether it is in a high temperature or severely cold environment. Pakrouh et al. [36] designed a liquid-cooled-TEC-PCM hybrid system, where PCMs are utilized to regulate the hot-side temperature of TECs; Their findings indicated that the improvement of coefficient of performance (COP) is closely related with the water flow rate and the usage of TECs. From the above, TECs can achieve efficient heat dissipation with a small input current. Their ability to achieve precise temperature control and fast thermal response renders them highly effective in overcoming the thermal management challenges of battery systems.

With the advancement of fast charging technology and the increasing demand for high energy density batteries, a great amount of heat may be generated within a short period during battery operation. An effective BTMS is urgently needed to dissipate heat during the fast discharging and charging process of batteries to prevent the battery from overheating. Accordingly, this work presents a novel BTMS that integrates VCs and TECs and establishes a comprehensive thermal-electric coupled model to evaluate its performance. Unlike previous studies that typically focus on single-component systems (e.g., TECs or VCs alone), this study systematically investigates the synergistic interactions between TECs and VCs under extreme 5 C high-rate discharge conditions. The integration of TECs and VCs leverages the complementary strengths of both technologies: VCs serve as highly thermal conductive passive heat spreaders, rapidly distributing localized heat and mitigating temperature gradients within the battery pack, while TECs provide precise and efficient active cooling by modulating heat removal based on thermal demand. This synergistic combination enables superior temperature control, reduced thermal gradients, and enhanced energy efficiency compared to systems using TECs or VCs alone. Moreover, considering that the TEC parameters highly influence the system's thermal performance, the influence of different parameters (e.g., input current, leg height, and air-side heat transfer coefficient) on the highest temperature and temperature difference of the BTMS is comprehensively investigated. A detailed parametric analysis reveals the nonlinear coupling effects of these factors, providing practical guidelines for TEC-VC system design. Meanwhile, the optimal operating conditions for the TEC are suggested based on the trade-offs between cooling power and energy efficiency. Ultimately, to emphasize the effectiveness of the TEC, two cases are proposed and contrasted: a BTMS with VCs and TECs (BTMS-VC&TEC) and a BTMS with only VCs (BTMS-VC).

2. Structure of the BTMS

The presented BTMS with TECs and VCs consists of four main components: a finned heat sink, four TECs, four VCs, and a battery pack, as depicted in Fig. 2. The VCs adopt a U-shaped configuration [37] and are categorized into two groups: short VC and long VC. The battery pack consists of three 12 A h square-shaped Lithium Iron Phosphate (LFP) battery cells [32] with a size of 90 mm × 70 mm × 27 mm. To achieve an effective reduction in battery temperature, each of the three battery cells

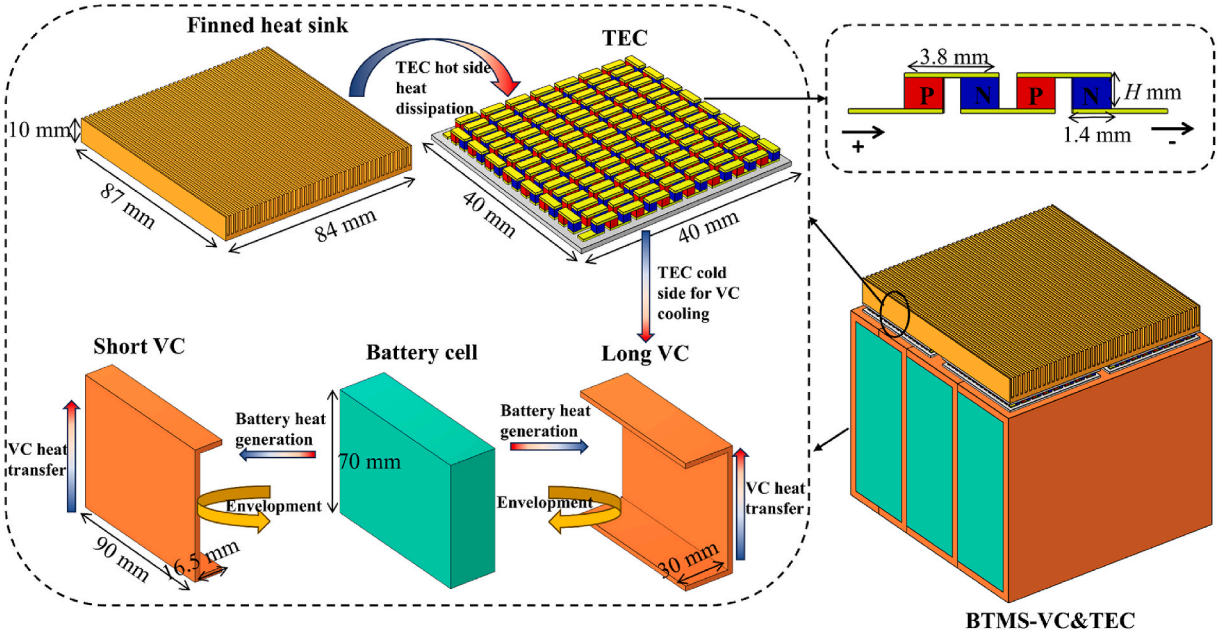

Fig. 2. Three-dimensional geometry schematic of the BTMS.

is surrounded by VCs. Two short VCs encase the leftmost battery cell, while a long VC encloses the second (or third) battery cell. The two VCs have the same lengths (90 mm) and heights (76 mm), and the widths of the short and long VCs are 16.5 mm and 30 mm respectively. Herein, the VCs are made up of two sections: the condenser and the evaporator. At the evaporator section, the working fluid absorbs the heat generated by the battery and subsequently evaporates. Afterward, the gaseous working fluid ascends to the top condensation section due to changes in internal pressure. After cooling by the TEC, the gaseous working fluid releases heat, thus achieving thermal transport between the condenser and evaporator. In this configuration, the VCs utilize their central and lower sections as an evaporator for heat absorption, and the upper section as a condenser for heat release [38]. To facilitate efficient heat dissipation and precise temperature control of the battery, four TECs are installed at the upper end of VCs. The TEC is composed of copper electrodes, ceramic plates, and both p-type and n-type thermoelectric legs. With a current passing through TECs, heat absorption at the bottom and heat release at the top occur in the TEC. Nevertheless, the heat accumulated at the TEC hot side may lead to excessive temperature gradients across the TEC, thus deteriorating its cooling performance. To address this issue, a finned heat sink measuring 84 mm × 87 mm × 10 mm is applied to the hot side of the TEC for heat dissipation, with a spacing and thickness of 1 mm for each fin. Although the integration of TECs and VCs introduces some additional mass, volume, cost, and energy consumption, the impact on the system's specific power and volumetric power density is limited. This is because the TEC modules are compact and lightweight compared to conventional liquid cooling systems, and the vapor chambers are designed as thin plates tightly coupled to the battery cells. The slight increases in system weight and volume are acceptable considering the substantial improvements in thermal regulation, efficiency, and operational flexibility. The material properties for aluminum, batteries [32], and VCs [39] are tabulated in Table 2, and those of the TEC are listed in Table 3, where Bi_2Te_3-based materials are employed for the thermoelectric legs, and the relevant values are obtained from Ref. [40]. In addition, the dimensional properties of the remaining physical models are given in Table 4.

3. Model development

3.1. Thermal-electric coupling model

Fig. 3 illustrates basic principles of the thermal-electric coupling model, encompassing the governing equations for both thermal and electrical fields. Variables like T are shared among multiple equations, interacting with each other throughout the system. For example, the heat produced by the battery [41] is initially conveyed to the evaporator section of VCs, then transferred from the evaporator to condenser, and finally transmitted to the cold end of TECs. When current is applied to TECs, the top and bottom of TECs will release and absorb heat, respectively. The bottom, which absorbs heat, becomes the cold end and takes away the heat from the condenser section of the VC, while the top is equipped with a finned heat sink for the effective dissipation of released heat from the top [42]. It's worth noting that to improve computational efficiency, the VCs are simplified as ideal solid models with uniform properties and ultra-high thermal conductivity [38]. This assumption may slightly overestimate heat diffusion performance, especially under transient or high heat flux conditions. Nonetheless, for the present system-level analysis of TEC parameter effects under high discharge rates, this simplification provides a reasonable approximation. Future work will focus on developing a detailed two-phase VC model that includes phase-change dynamics, capillary effects, and transient thermal behavior. The whole system obeys the principle of energy conservation [43], where the heat generated by the battery and the Joule heat induced by the electric field are treated as energy source terms in the governing equations. Additionally, the solid regions involving electric current adhere to electric field conservation and current continuity [44]. More comprehensive details regarding this model are documented in Ref. [45]. Even at high discharge rates, the given BTMS demonstrates excellent capability in meeting the heat dissipation demands. To accentuate its benefits, this paper adopts a 5 C discharge rate, with a heat generation power of 21.6 W [32]. Furthermore, all batteries are assumed as homogenous solid blocks with uniform thermal properties.

Table 2
Detailed material parameters for batteries, heat sink, and VCs.

Property	Battery [32]	Heat sink	VC [39]
Specific heat capacity (J/(kg·K))	1150	900	381
Density (kg/m^3)	1838.2	2700	8978
Thermal conductivity (W/(m·K))	15.3, 15.3, 0.9 (k_x, k_y, k_z)	238	2000

3.2. Boundary conditions

Numerical calculations of the thermal-electric coupling model described above are conducted using the commercial software COMSOL. Furthermore, necessary boundary conditions need to be established during simulations. For air-cooled heat sinks, the heat transfer coefficient (h_{air}) typically ranges from 10 to 50 W/(m^2·K) [42]. Therefore, in both cases (BTMS-VC&TEC and BTMS-VC), h_{air} is set as 30–50 W/(m^2·K) with intervals of 2.5 W/(m^2·K) to study the influence of air cooling on the BTMS performance, with the ambient temperature (T_{air}) of 293.15 K. Thermal loss boundary conditions are applied to other BTMS surfaces in contact with the ambient environment, incorporating a heat loss coefficient of 10 W/(m^2·K).

In the thermoelectric domain, the surface of the copper conductor where the current enters is specified with a normal current density boundary condition, whereas the surface where the current exits is assigned a ground boundary condition. Under the above conditions, numerical calculations of the thermal-electric coupling model can be completed.

3.3. Parameter definitions

The coefficient of performance (COP) and cooling power (Q_c) are two critical parameters used to evaluate the cooling performance of a TEC, thereby reflecting its application potential in thermal management. Specifically, Q_c represents the heat absorbed at the cold side of the TEC, while the corresponding heat is dissipated from the hot side, denoted as Q_h. According to Ref. [46], the calculations for Q_c and Q_h of the TEC are as follows:

$$Q_c = \alpha I_{TEC} T_c - \frac{1}{2} I_{TEC}^2 R_{TEC} - \lambda_{TEC}(T_h - T_c) \quad (1)$$

$$Q_h = \alpha I_{TEC} T_h - \frac{1}{2} I_{TEC}^2 R_{TEC} - \lambda_{TEC}(T_h - T_c) \quad (2)$$

where, T_h and T_c are respectively temperatures on the hot and cold ends of the TEC; I_{TEC} is the current of TECs, R_{TEC} denotes the overall electrical resistance of all thermoelectric legs, λ_{TEC} is the heat conduction across the entire TEC.

Therefore, the combination of equations (1) and (2) yields the power input of the TEC, which is:

$$P_{in} = Q_h - Q_c = I_{TEC}^2 R_{TEC} + \alpha I_{TEC}(T_h - T_c) \quad (3)$$

Then, the COP of the TEC is defined as the ratio of the heat absorbed at the cold side (Q_c) to the input electrical power (P), which can be expressed as:

Table 3
Parameters of each component of the TEC [40].

	Seebeck coefficient (μV/K)	Thermal conductivity (W/(m·K))	Electrical resistivity (10^{-5} Ω·m)	Size (L × W × H mm^3)
n-type legs	$7.393\times10^{-11}T^2-2.500\times10^{-7}T-8.494\times10^{-5}$	$1.870\times10^{-5}T^2-1.447\times10^{-2}T+3.680$	$0.657T^2-7.136\times10^{2}T+2.463\times10^{5}$	1.7 × 1.7 × 1.4
p-type legs	$-1.593\times10^{-9}T^2+1.364\times10^{-6}T-7.062\times10^{-5}$	$1.071\times10^{-5}T^2-8.295\times10^{-3}T+2.625$	$1.311T^2-1.364\times10^{3}T+4.023\times10^{5}$	1.7 × 1.7 × 1.4
copper electrodes	–	400	1.67×10^{-3}	4.2 × 1.7 × 0.2
ceramic plates	–	22	–	40 × 40 × 0.8

Table 4
The dimensional properties of other physical models.

	Battery	Finned heat sink	Long VC	Short VC
Size (L × W × H mm^3)	90 × 27 × 70	87 × 84 × 10	90 × 30 × 76	90 × 16.5 × 76

$$\mathrm{COP}=\frac{Q_c}{P_{in}} \tag{4}$$

In addition, the maximum temperature of the battery pack refers to the highest temperature among all battery surfaces, and the temperature difference is calculated as the difference between the maximum and minimum surface temperatures.

3.4. Grid independence examination

To ensure the accuracy of the simulation results, a mesh independence study is carried out. The computational grids are generated using COMSOL, as shown in Fig. 4. Five groups of progressively increased grids are used: 127733, 218500, 437940, 575354, and 1012654. The temperature difference and maximum temperature of batteries under various mesh configurations are presented in Fig. 5. The maximum temperature and temperature difference converge at 575354 grids, with a negligible difference of only 0.01 K compared to the finer mesh (1012654 grids). This confirms that the chosen grid density effectively captures the thermal gradients and coupled heat transfer phenomena, balancing accuracy and computational efficiency.

3.5. Model verification

To validate the precision of the established electric-thermal coupling model, the work utilizes experimental data from previously published works for model validation. The physical model of the BTMS, integrating U-shaped VC and air cooling as described in Ref. [47] is established. Subsequently, a finite element model of the system has been developed and predicted its performance using the given model. In the numerical simulation process, to ensure the accuracy of the numerical simulation and eliminate the influence of unrelated variables, the boundary conditions were established based on the experimental setup reported in Ref. [47]. Fig. 6 presents a comparison between the simulated maximum temperatures and the corresponding experimental data. The simulation results exhibit strong consistency with the experimental measurements, with a maximum deviation of approximately 1.5 K. This discrepancy is primarily attributed to the simplification of the VC model, which neglects internal vapor-liquid phase change dynamics; the uniform heat generation assumption, which omits localized hotspots and dynamic resistance changes; and minor experimental uncertainties, including sensor placement, thermal lag, and data acquisition errors. Overall, the good agreement between simulation and experimental results provides strong support for the accuracy and reliability of the established

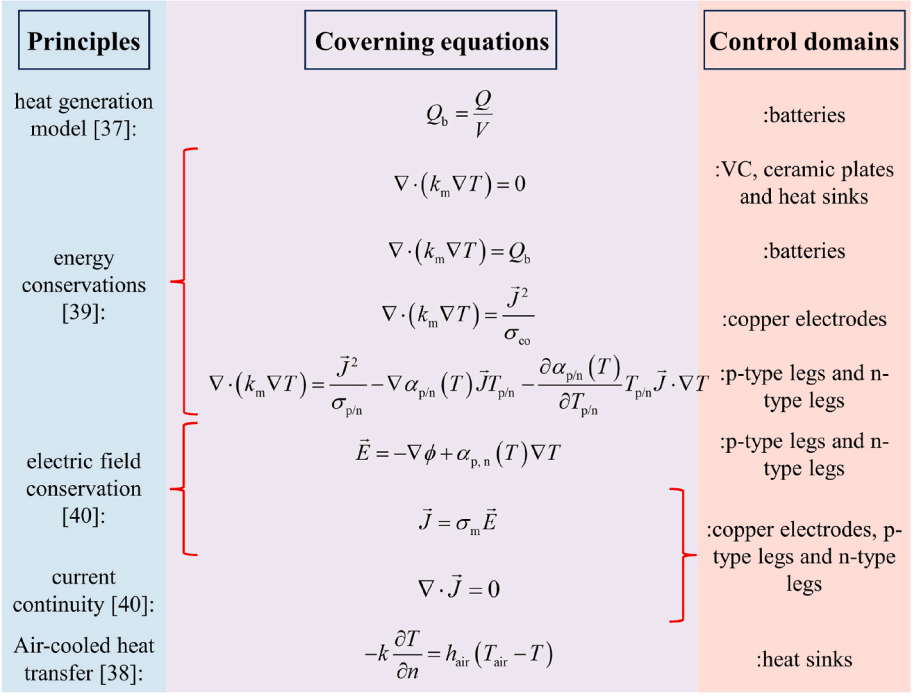

Fig. 3. Basic theory of the thermal-electric coupling model.

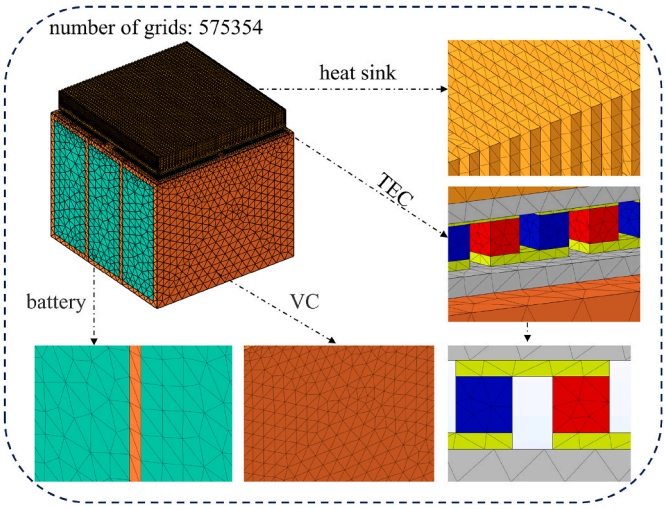

Fig. 4. Mesh model of the BTMS.

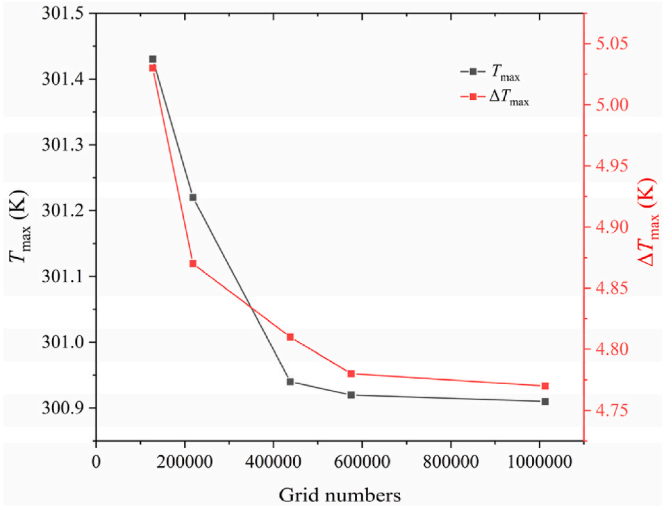

Fig. 5. Variation of temperature difference and maximum temperature with grid numbers.

thermal-electric coupled model.

In addition, to further highlight the reasonability of the developed model, the TEC modeling part is also verified. The data of cooling power from Ref. [48] are used to perform the comparison, under the same TEC model and boundary conditions, as shown in Fig. 7. The results obtained in this study align well with those reported in Ref. [48], with a maximum deviation of approximately 7.95 %. This error may primarily arise from the fact that certain detailed conditions in Ref. [48], such as thermal and electrical contact resistances at the interfaces within the TEC module, are not fully considered in this study due to the lack of corresponding experimental data. Additionally, the assumption of constant material properties further contributes to the discrepancy at higher currents. The validation of both the overall BTMS and the TEC module confirms that the proposed electro-thermal model reliably predicts the thermal behavior of the TEC-integrated system.

4. Results and discussion

This study conducts an in-depth investigation into the cooling performance of the TEC and the thermal characteristics of the BTMS. Based on the criteria outlined in Ref. [7], the battery's operating temperature is constrained to remain below 313.15 K, with a maximum permissible

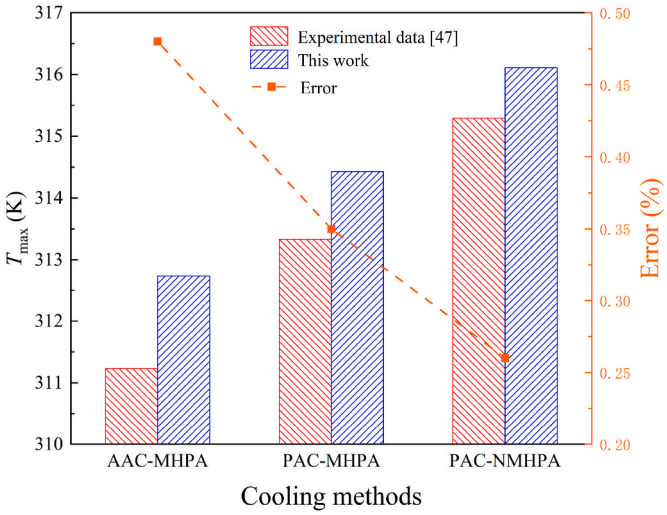

Fig. 6. Experimental validation of the proposed model. (Note: NMHPA for the no micro heat pipe array, AAC for the active air cooling, PAC for the passive air cooling, and MHPA for the micro heat pipe array).

temperature difference of 5 K. Additionally, the minimum temperature should be higher than 293.15 K [49]. Generally, the lower the height of the thermoelectric leg, the lower the internal resistance, allowing the TEC to produce greater cooling power with the same current input. However, in practical battery thermal management applications, a reduced height increases the temperature difference across the TEC, which negatively impacts its cooling performance. Therefore, a comprehensive parametric study for the thermoelectric-based BTMS is essential.

4.1. The numerical results of a single TEC

Fig. 8(a) illustrates the temperature boundary conditions of the TEC, where the hot side is maintained at 313.15 K and the cold side at 293.15 K. The corresponding distributions of temperature, voltage, and current density are depicted in Fig. 8(b)–(d). As shown in Fig. 8(b), the temperature gradient is mainly concentrated within the thermoelectric legs due to their relatively low thermal conductivity compared to other structural components. When current flows through the TEC, holes in the p-type leg (red in Fig. 8(a)) and electrons in the n-type leg (blue in Fig. 8(a)) move from the cold end to the hot end, resulting in heat absorption at the cold side and release at the hot side. Concurrently, the temperature gradient induces carrier movement in the opposite direction. According to Eq. (1), an increasing temperature difference between the TEC's sides reduces its cooling efficiency. Therefore, to ensure effective operation under large temperature gradients, a suitable input current is essential. The voltage distribution across the TEC, as shown in Fig. 8(c), provides critical insight into the device's internal electrical behavior and its impact on thermal performance. The electric potential increases smoothly from the ground terminal to the input terminal, reaching 6.58 V at an input current of 3 A. This voltage distribution reflects the direction of current flow that drives the Peltier effect, the core mechanism responsible for heat absorption at the cold side and heat release at the hot side of the thermoelectric module. The corresponding electrical power input, calculated as the product of voltage and current, is 19.74 W, which is slightly lower than the theoretical value obtained from Eq. (3). Fig. 7(d) shows the highest current density at the copper electrode, attributed to copper's excellent electrical conductivity. Furthermore, the simulation outputs provide the necessary data for calculating the cooling capacity and COP.

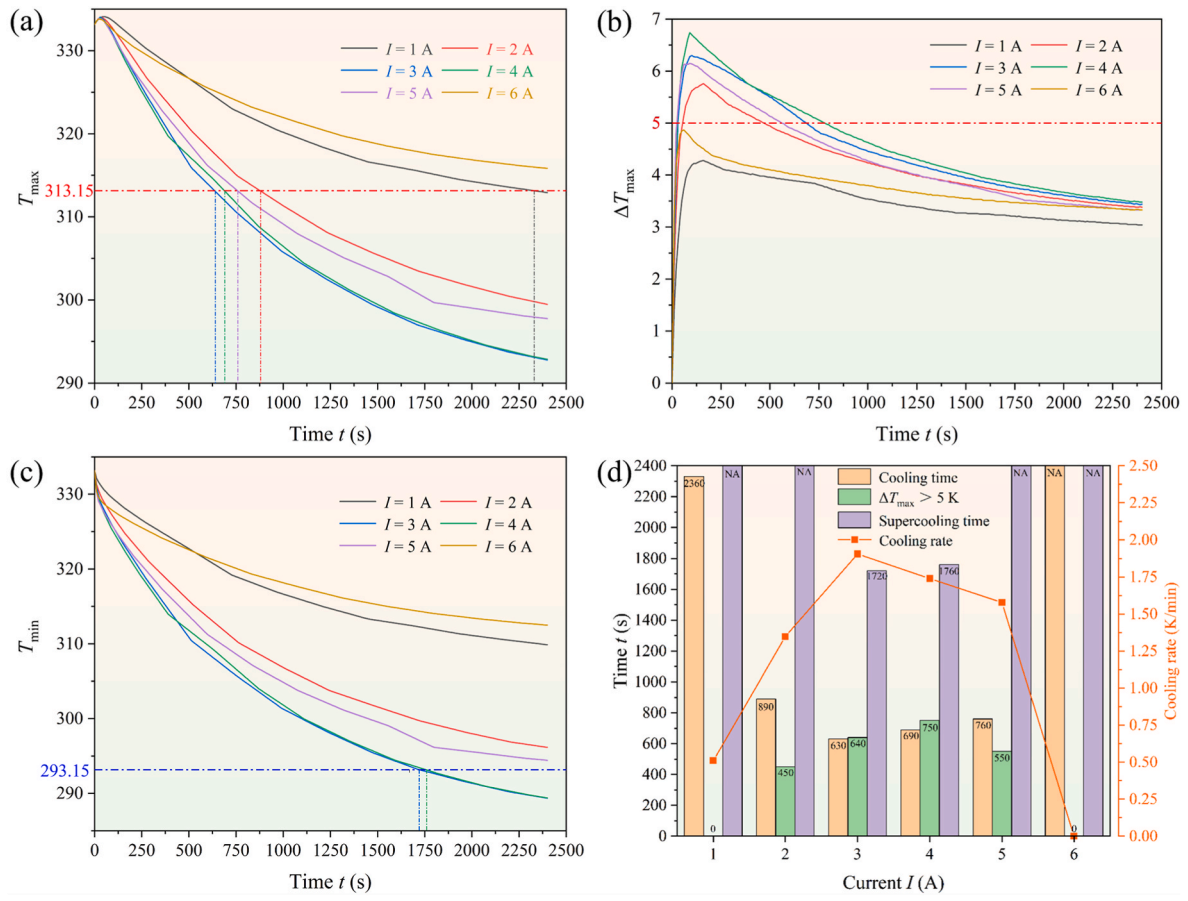

Fig. 7. Validation of the TEC modeling part.

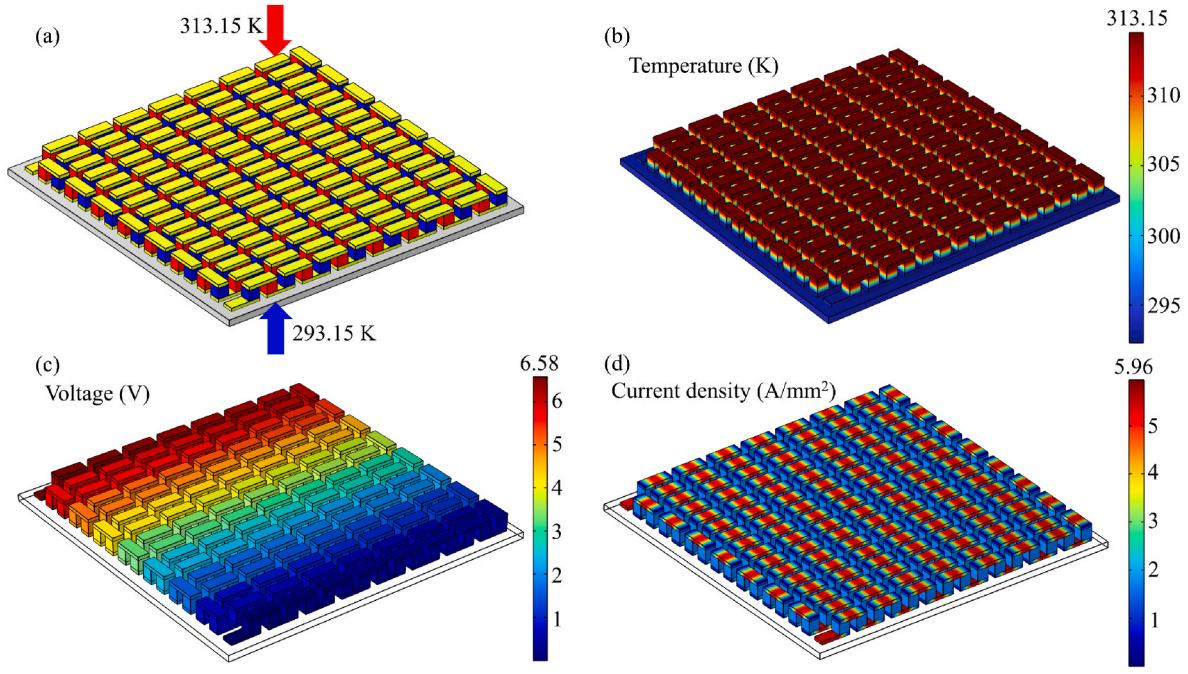

Fig. 8. Numerical simulation results of a single TEC when the current input is 3 A. (a) Three-dimensional geometry and temperature boundary conditions of the TEC; (b) Temperature distributions of the TEC; (c) Voltage distributions of the TEC; (d) Current density distributions of the TEC.

4.2. Effect of leg height on the TEC cooling performance

Fig. 9 demonstrates the impact of different leg heights on the cooling performance of the TEC under varying input currents. In this case, the cold end temperature of the TEC is set to 293.15 K, and the hot end temperature to 313.15 K. With the input current increases, Q_c initially rises, then decreases, as shown in Fig. 9(a). This nonlinear behavior is governed by the interplay between the Peltier effect, Joule heating, and thermal conduction: at low currents, Q_c increases linearly with current due to enhanced Peltier cooling, but at higher currents, Joule heat generated inside the thermoelectric legs and parasitic heat conduction from the hot to cold side reduce the net cooling effect—leading to a decline in Q_c. Specifically, at a leg height of 1.4 mm, Q_c increases by 29.6 W as the input current rises from 1.5 A to 7.5 A, while the COP remains at only 0.3 at 7.5 A. Additionally, as the leg height decreases, Q_c increases, and the effective operating span of the input current of the TEC also increases. From Fig. 9(b), it can be observed that when the input current is lower than 1.5 A, Q_c is relatively small while P_{in} is large, leading to a quite small COP. With the input current increases, COP initially rises and then declines, with the decreasing trend being gradually slowing down. Furthermore, with the reduction in the leg height, a significant increase in COP is observed. To achieve a balance between Q_c and COP, it is recommended to set the TEC input current below 4 A.

This section further analyzes the influence of the leg height on the TEC voltage distribution under a 3 A input current, as shown in Fig. 10. It can be noticed that as the thermoelectric leg height decreases, the voltage also decreases, attributed to the decreased internal resistance. The reduction in internal resistance results in a decrease in Joule heating, which in turn leads to an increase in the Q_c. Moreover, with the leg height increases from 0.8 mm to 1.6 mm, the voltage rises by 3.35 V. The growth in voltage value induces an increase in input power, hence resulting in a decrease in COP. It seems that the leg height of the TEC should be minimized to optimize cooling performance.

4.3. Effect of leg height on the BTMS thermal performance

The previous section focused only on a single TEC with a fixed temperature difference between the hot and cold ends, without considering its application in the BTMS. Therefore, this section investigates the practical performance of TECs within the BTMS using numerical simulations. Considering the great influence of the leg height on the TEC cooling performance, a corresponding study is performed, as shown in Fig. 11. When the air convective heat transfer coefficient is fixed at 50 W/(m^2·K), the maximum battery temperature first decreases and then increases with rising input current (Fig. 11(a)). This behavior stems from the competing effects of Peltier cooling (linear in current) and Joule heating (quadratic in current). At lower currents, Peltier cooling dominates, reducing battery temperature. However, as current further increases, Joule heating grows more rapidly, eventually overtaking Peltier cooling and degrading the TEC's net cooling capacity. When the current is 1 A, the higher the leg height, the larger the battery maximum temperature. This is because under low current conditions, the TEC generates limited cooling power, causing the temperature gradient between its legs to remain nearly uniform despite differences in leg height. At lower leg heights, the cooling power Q_c increases, leading to a reduction in battery pack temperature. Within the 1.5–2.5 A range, the maximum battery temperature inversely correlates with leg height. The underlying mechanism is that elevated input currents significantly widen the temperature difference between the TEC's hot and cold ends, making shorter legs more effective at heat extraction. Although the TEC with a lower height may produce a higher cooling power, it can only operate under a relatively low temperature difference, and thus the increased temperature difference hinders the cooling performance of TECs. It is worth noting that this trend will change as the current increases further. With the current continues to rise, the maximum temperature with a larger leg height will gradually exceed that of the battery pack with a smaller height. It can be observed that when the input current is 3 A and the height of thermoelectric legs is 1.4 mm, the BTMS achieves the lowest maximum temperature, which is 300.94 K.

As shown in Fig. 11(b), increased current magnitude correlates with enhanced battery surface cooling, resulting in more pronounced temperature gradients. However, excessive current results in a decrease in TEC cooling power, causing the maximum temperature difference of batteries to increase initially and then decrease with the input current, contrary to the trend observed in the maximum temperature. Additionally, with an input current of 3 A, compared with the situation of 0.8 mm, the temperature difference of the BTMS with a height of 1.4 mm is only increased by 0.04 K, while the maximum temperature is decreased by 4.78 K. Therefore, the leg height of TECs is suggested to be 1.4 mm. In summary, selecting the optimal leg height involves a trade-off between thermal efficiency and the ability to withstand temperature gradients. In the present configuration, the battery pack reaches its lowest maximum temperature at a leg height of 1.4 mm under a 3 A input current. This indicates a favorable balance between performance and adaptability, yielding a higher COP while maintaining sufficient thermal regulation capability. Therefore, the 1.4 mm leg height is identified as the optimal configuration.

To gain deeper insight into the thermal distribution within the BTMS, numerical simulations are conducted under various TEC input currents, as shown in Fig. 12. In these simulations, the air convective heat transfer coefficient is held constant at 50 W/(m^2·K), and the thermoelectric leg height is set to 1.4 mm. The results reveal that as the input current increases, the temperature of the finned heat sink also rises. Specifically, at an input current of 3 A, the heat sink reaches 335 K, primarily due to the

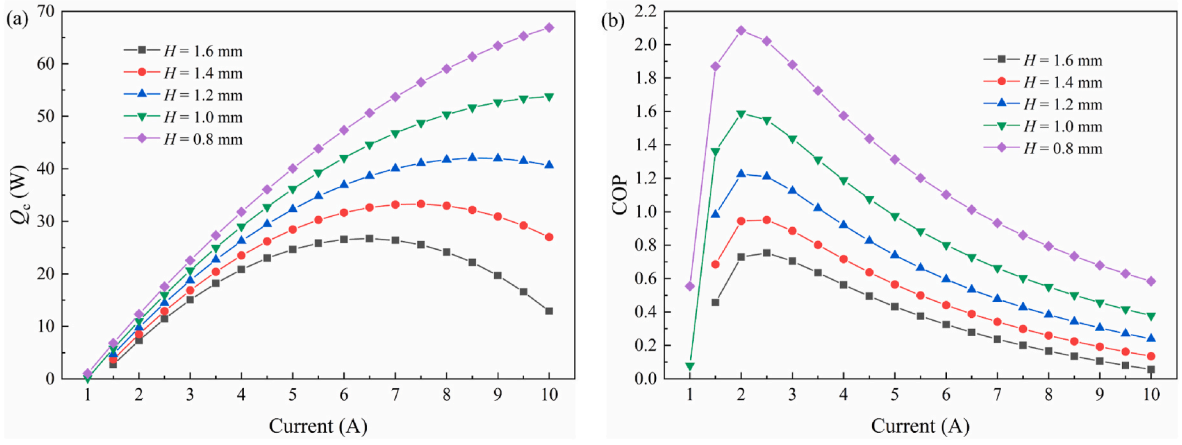

Fig. 9. Effect of leg height on TEC performance under various input currents. (a) Q_c; (b) COP.

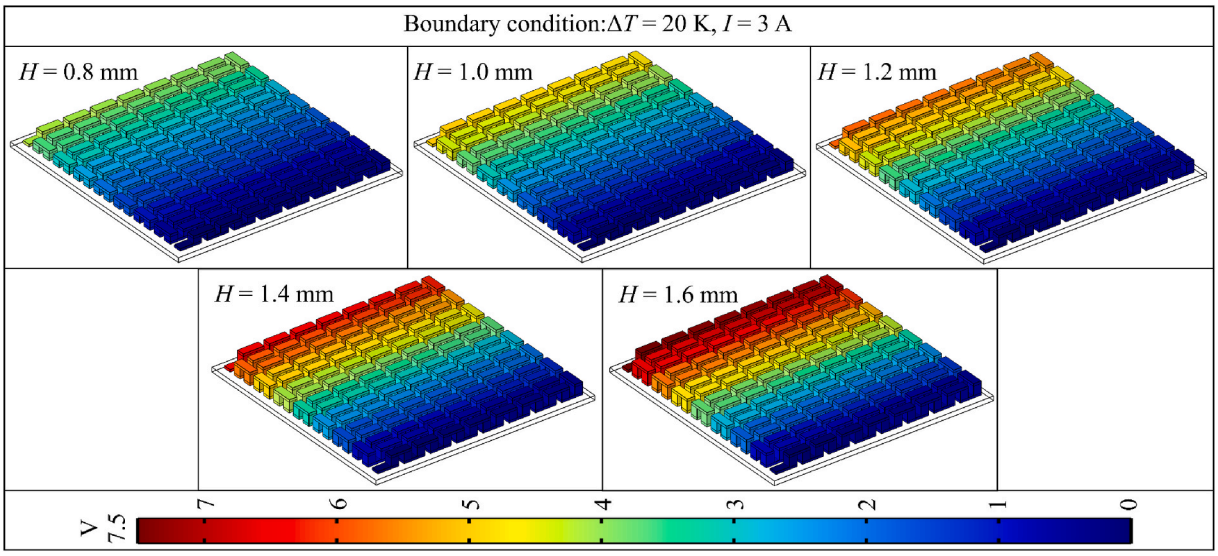

Fig. 10. Voltage distribution of the TEC at different leg heights.

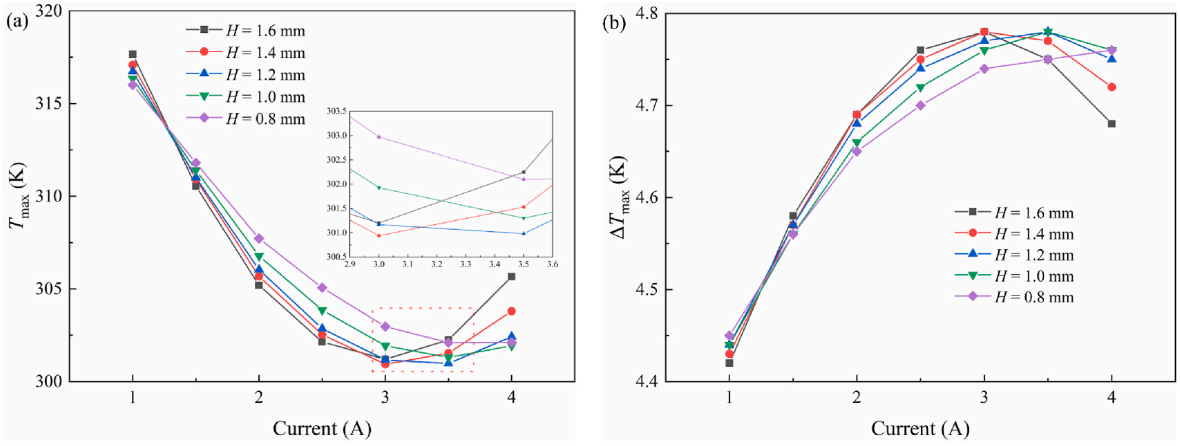

Fig. 11. Influence of leg height on the thermal behavior of the BTMS under various input currents. (a) T_{max}; (b) ΔT_{max}.

enhanced Peltier heating effect on the TEC's hot side. Meanwhile, the cold side of the TEC provides more effective cooling, resulting in a lower battery temperature. Between 1 A and 3 A, the battery's maximum temperature drops by 16.15 K. However, further increasing the current beyond 3 A leads to a gradual rise in battery temperature, mainly due to the decline in cooling efficiency caused by the enlarged temperature gradient across the TEC. Therefore, while a moderate increase in input current can effectively enhance TEC cooling performance and reduce battery temperature, excessively high input currents not only lead to significant energy consumption but also impair thermal regulation. Based on the simulation results in Fig. 11, the optimal current range for maintaining efficient TEC operation lies between 2.5 A and 3.5 A.

4.4. *Effect of air cooling and comparison between two configurations*

To evaluate the TEC's effectiveness in battery thermal management, two BTMS configurations with and without TECs are compared in this section, and the influence of varying air convection heat transfer coefficients is investigated, as shown in Fig. 13. Here, the leg height and input current are set as the optimal values of 1.4 mm and 3 A respectively.

As shown in Fig. 13(a), increasing the air convection heat transfer coefficient leads to a reduction in the maximum temperature for both BTMS configurations. In the BTMS-TEC&VC setup, the incorporation of TECs significantly boosts the air-cooling effectiveness of the finned heat sink, resulting in a more pronounced temperature drop. Specifically, when the heat transfer coefficient reaches 50 W/(m^2·K), the maximum temperature of the BTMS-TEC&VC is 13.58 K lower than that of the BTMS-VC. Notably, the BTMS-VC configuration fails to keep the battery temperature below the safety limit of 313.15 K, highlighting its insufficient cooling capacity. For the BTMS-TEC&VC configuration, even under a high discharge rate of 5 C, the system can effectively maintain battery temperatures within the safe operating range with a 3 A TEC input current. This demonstrates that, while the integration of TEC increases energy consumption and cost, its enhanced thermal regulation capabilities are critical for ensuring the safety and performance of high energy density battery packs, enabling effective temperature control under various operating conditions. In contrast, Fig. 13(b) reveals a positive correlation between h_{air} and temperature differential for both systems, with temperature differential increasing progressively with higher convection coefficients. The temperature difference in the BTMS-TEC&VC configuration is marginally higher than that in the BTMS-VC, with a maximum disparity of just 0.29 K at h_{air} = 50 W/(m^2·K). This slight increase is due to the enhanced cooling capability of the TEC, which lowers the outer surface temperature of the battery, thereby amplifying the temperature gradient within the module. Overall, the

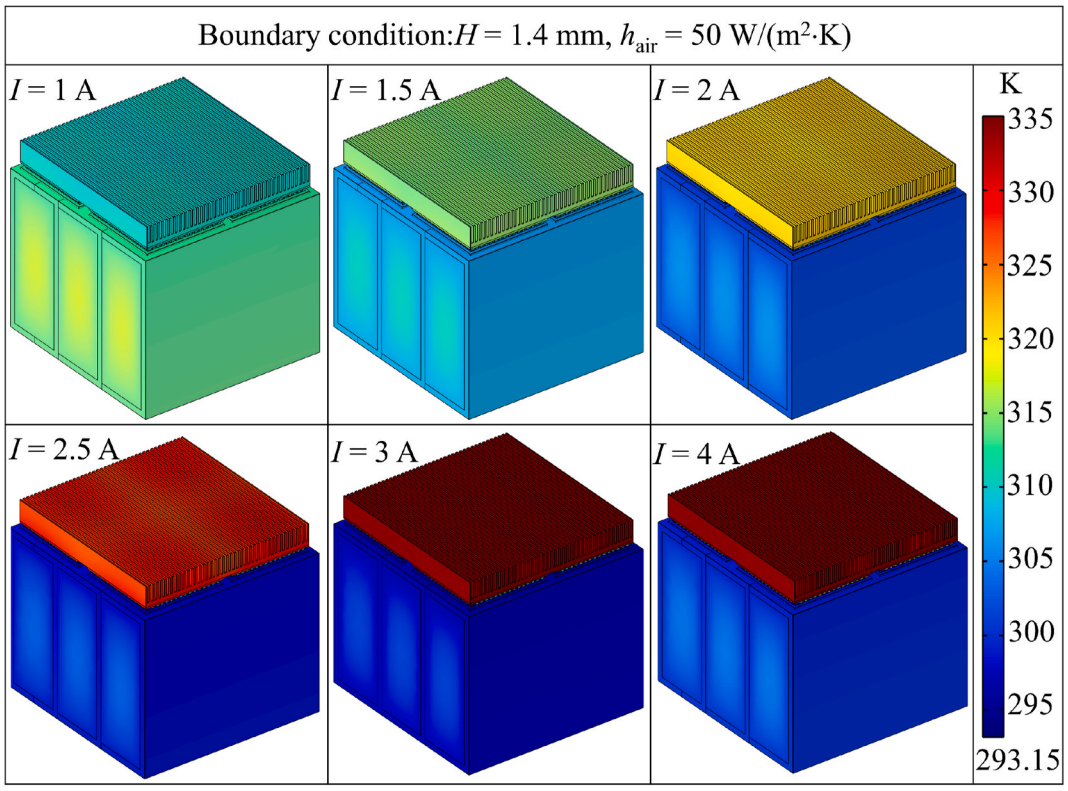

Fig. 12. Temperature distribution of BTMS under different input currents.

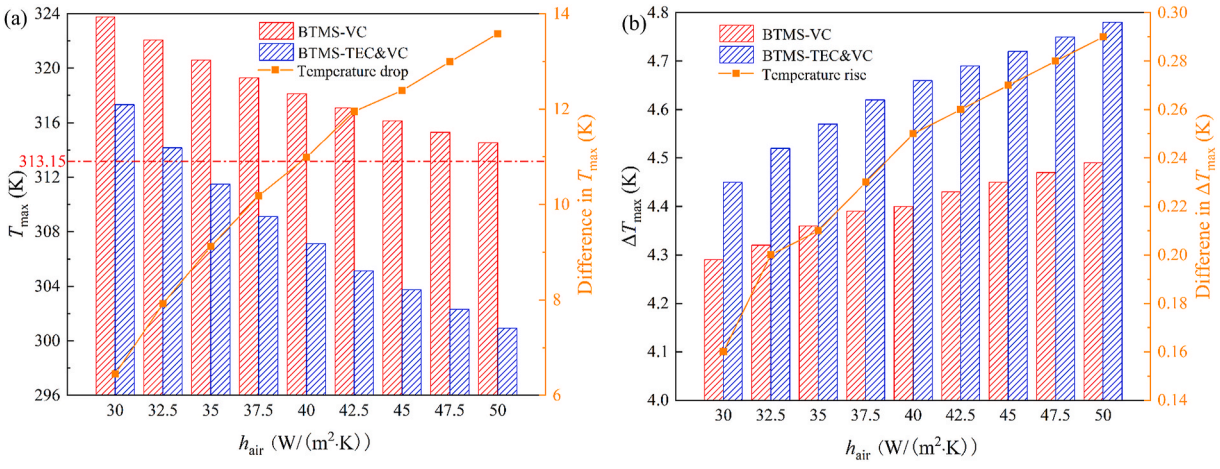

Fig. 13. Effect of air cooling and comparison between two configurations. (a) T_{max}; (b) ΔT_{max}.

integration of TECs significantly reduces the battery's peak temperature. Although a minor rise in temperature difference is observed, it remains below 5 K, thus satisfying the BTMS thermal management requirements.

In summary, increasing the convective heat transfer coefficient further reduces the maximum battery temperature but leads to a slight increase in temperature difference. Considering that the BTMS-TEC&VC configuration already demonstrates excellent thermal performance at h_{air} = 50 W/(m^2·K), further improvements in thermal performance become marginal beyond this point. Moreover, increasing the coefficient beyond 50 W/(m^2·K) would significantly raise energy consumption [50]. Therefore, by comprehensively evaluating cooling effectiveness and energy efficiency, 50 W/(m^2·K) is identified as the optimal convective heat transfer coefficient.

5. Conclusions

This study addresses the thermal management challenges of battery systems under high discharge rates (5 C) by proposing a novel BTMS configuration integrating TECs and VCs. The hybrid TEC-VC design significantly improves thermal regulation to maintain optimal battery operating temperatures. In the proposed BTMS, the utilization of VCs is able to effectively lower the temperature difference, and the utilization of TECs can notably alleviate the maximum temperature of batteries. In addition, considering the high sensitivity of TEC parameters to the system's thermal performance, the effect of different parameters on the maximum temperature and temperature uniformity of the BTMS is comprehensively analyzed, and the optimal conditions for the TEC are suggested, including the leg height, current input, and air cooling heat

transfer coefficient. Meanwhile, a thermal-electric coupling model for the BTMS is established to forecast its thermal performance. The summarized results are as follows.

(1) For a single TEC, both Q_c and COP experience an initial ascent followed by a subsequent decline with an augmentation in the TEC current input. To strike an optimal balance between Q_c and COP, it is advisable to constrain the TEC current input to not exceed 4 A, and the leg height should remain relatively low to ensure a high COP. However, the situation for the thermal management applications of the TEC is quite different from the individual TEC.
(2) Although the individual TEC with a lower leg height may produce a higher cooling power, it can only operate at a relatively low temperature difference, and the increased temperature difference hinders the cooling performance of TECs with a relatively low leg height, thereby leading to poor thermal behavior of the BTMS.
(3) As the input current to the TEC increases, the battery's maximum temperature initially decreases and then rises, while the temperature difference exhibits the opposite trend. In the current range of 1.5 A–2.5 A, a greater leg height results in a lower maximum temperature. When the current reaches 3 A, a leg height of 1.4 mm achieves the lowest maximum temperature of 300.94 K, with only a slight increase in the temperature difference.
(4) As the air cooling heat transfer coefficient increases, a continuous decrease in the maximum temperature is observed, accompanied by a gradual rise in the temperature difference. Compared to the BTMS without TECs, integrating TECs reduces the maximum temperature by 13.58 K at a heat transfer coefficient of 50 W/(m^2·K), while the associated increase in temperature difference remains minimal at just 0.29 K.
(5) Future work will extend the analysis to include transient thermal performance under dynamic operating conditions and develop adaptive TEC control strategies that allocate specific TECs to groups of batteries and dynamically adjust input current based on real-time temperature feedback, ensuring efficient, energy-saving, and uniform temperature regulation for large battery packs across diverse scenarios.

CRediT authorship contribution statement

Ding Luo: Project administration, Investigation, Conceptualization, Writing – original draft, Methodology, Funding acquisition. **Zihao Wu:** Writing – original draft, Validation, Visualization. **Haifeng Wu:** Validation, Investigation, Software, Data curation. **Hao Chen:** Writing – review & editing, Resources, Supervision, Funding acquisition. **Peng Zhang:** Formal analysis, Data curation. **Bingyang Cao:** Supervision, Resources, Writing – review & editing, Software, Project administration.

Declaration of competing interest

The authors declare that they have no known competing financial interests or personal relationships that could have appeared to influence the work reported in this paper.

Acknowledgments

This work was supported by the National Natural Science Foundation of China (52306017), and the Fundamental Research Funds for the Central Universities (CHD300102385201).

Data availability

Data will be made available on request.

References

[1] Zhou Y, Zheng S, Hensen JLM. Machine learning-based digital district heating/cooling with renewable integrations and advanced low-carbon transition. Renew Sustain Energy Rev 2024;199:114466.
[2] Cao J, Wu H, Zhang D, Luo D, Zhang L, Yang X, et al. In-situ ultrafast construction of zinc tungstate interface layer for highly reversible zinc anodes. Angew Chem Int Ed 2024:e202319661. n/a.
[3] Cao J, Sun M, Zhang D, Zhang Y, Yang C, Luo D, et al. Tuning vertical electrodeposition for dendrites-free zinc-ion batteries. ACS Nano 2024.
[4] Luo D, Wu Z, Yan Y, Sun Z, Yang L, Cao B. Performance analysis of a battery thermal management system combining thermoelectric, composite phase change material, and liquid cooling under extreme operating conditions. J Energy Storage 2024;95:112679.
[5] Jilte R, Afzal A, Khan SA, Asif M, Venkatesan EP, Munimathan A. Cooling performance of a Li-ion cylindrical battery pack with liquid circulating pipes embedded in phase change material. J Energy Storage 2024;87:111335.
[6] Lu F, Chen W, Hu S, Chen L, Sharshir SW, Dong C, et al. Achieving a smart thermal management for lithium-ion batteries by electrically-controlled crystallization of supercooled calcium chloride hexahydrate solution. Appl Energy 2024;364:123180.
[7] Liang K, Zhang Y, Wang W, Gao C, Chen H, Li K, et al. Performance analysis and multi-objective optimization of refrigerant-based integrated thermal management system for electric vehicles. Appl Therm Eng 2024;244:122707.
[8] Kan R, Xu Y, Chen R, Jiang M, Fu B, Song C, et al. Thermal effects of solid-state batteries at different temperature: recent advances and perspectives. Energy Storage Mater 2024;68:103366.
[9] Patel JR, Rathod MK. Influence of battery cell spacing on thermal performance of phase change material filled lithium-ion battery pack. Energy 2024;291:130389.
[10] Xiong R, Li X, Li H, Zhu B, Avelin A. Neural network and physical enable one sensor to estimate the temperature for all cells in the battery pack. J Energy Storage 2024;80:110387.
[11] Yang L, Zhou F, Sun L, Wang S. Thermal management of lithium-ion batteries with nanofluids and nano-phase change materials: a review. J Power Sources 2022;539:231605.
[12] Subramanian M, Solomon JM, Raja V, Stanislaus Arputharaj B, Shaik S, Saleel CA, et al. Experimental studies and comprehensive computational investigations on composites-based phase change material for battery thermal management systems in electric vehicles. J Energy Storage 2024;82:110471.
[13] Hou J, Wu X, Chen K, Dong Y. A direct optimization strategy based on field synergy equation for efficient design of battery thermal management system. Int J Heat Mass Tran 2022;184:122304.
[14] Yu Z, Zhang J, Pan W. A review of battery thermal management systems about heat pipe and phase change materials. J Energy Storage 2023;62:106827.
[15] Kaur I, Singh P. Progress in minichannel-based thermal management of lithium-ion batteries. Renew Sustain Energy Rev 2023;187:113711.
[16] Fathimathul Faseena AM, Sreekumar A. Advances, perspectives and challenges in phase change material based battery thermal management: a comprehensive review. J Energy Storage 2025;113:115644.
[17] Dwivedi A, Kumar R, Goel V, Rana S, Kumar R, Kumar A. A comprehensive review on heat pipe-assisted hybrid battery thermal management strategies: opportunities, challenges and its future aspects. J Energy Storage 2025;112:115475.
[18] Daniels RK, Langeh H, Kumar V, Chouhan SS, Prabhakar A. Faulty cell prediction accuracy comparison of machine learning algorithms using temperature sensor placement optimization approach in immersion cooled Li-ion battery modules. Appl Energy 2024;367:123299.
[19] Keyhani-Asl A, Perera N, Lahr J, Hasan R. Porous media and foam application in battery thermal management systems: a comprehensive review focused on its impact, numerical modeling, and experimental preparation. J Energy Storage 2024;93:112306.
[20] Luo D, Wu Z, Jiang L, Yan Y, Chen W-H, Cao J, et al. Realizing rapid cooling and latent heat recovery in the thermoelectric-based battery thermal management system at high temperatures. Appl Energy 2024;370:123642.
[21] Vikram S, Vashisht S, Rakshit D, Wan MP. Recent advancements and performance implications of hybrid battery thermal management systems for electric vehicles. J Energy Storage 2024;90:111814.
[22] Jhariya M, Dewangan AK, Moinuddin SQ, Kumar S, Ahmad A, Yadav AK. Research progress on efficient battery thermal management system (BTMs) for electric vehicles using composite phase change materials with liquid cooling and nanoadditives. J Therm Anal Calorim 2024;149:13653–80.
[23] Feng R, Huang P, Tang Z, He Y, Bai Z. Experimental and numerical study on the cooling performance of heat pipe assisted composite phase change material-based battery thermal management system. Energy Convers Manag 2022;272:116359.
[24] Narimani M, Emami SA, Banazadeh A, Modarresi A. A unified thermal management framework for electric vehicles: design and test bench implementation. Appl Therm Eng 2024;248:123057.
[25] Monika K, Punnoose EM, Datta SP. Multi-objective optimization of cooling plate with hexagonal channel design for thermal management of Li-ion battery module. Appl Energy 2024;368:123423.
[26] Tran T-H, Harmand S, Desmet B, Filangi S. Experimental investigation on the feasibility of heat pipe cooling for HEV/EV lithium-ion battery. Appl Therm Eng 2014;63:551–8.
[27] Jouhara H, Delpech B, Bennett R, Chauhan A, Khordehgah N, Serey N, et al. Heat pipe based battery thermal management: evaluating the potential of two novel battery pack integrations. International Journal of Thermofluids 2021;12:100115.

[28] Ye Y, Saw LH, Shi Y, Tay AAO. Numerical analyses on optimizing a heat pipe thermal management system for lithium-ion batteries during fast charging. Appl Therm Eng 2015;86:281–91.
[29] Luo D, Zhao Y, Cao J, Chen W-H, Zhao Y, Cao B. Performance analysis of a novel thermoelectric-based battery thermal management system. Renew Energy 2024;224:120193.
[30] Siddique ARM, Bozorgi M, Venkateshwar K, Tasnim S, Mahmud S. Phase change material-enhanced solid-state thermoelectric cooling technology for food refrigeration and storage applications. J Energy Storage 2023;60:106569.
[31] He Z, Zuazua-Ros A, Martín-Gómez C. Current-dependent temperature change model of a thermoelectric window frame. Appl Therm Eng 2024;247:123081.
[32] Luo D, Wu Z, Yan Y, Cao J, Yang X, Zhao Y, et al. Performance investigation and design optimization of a battery thermal management system with thermoelectric coolers and phase change materials. J Clean Prod 2024;434:139834.
[33] Luo D, Chen H, Chen W-H, Zhang X, Geng L, Jiang W, et al. Interdependent optimization strategies for material, module, and system designs in thermoelectric devices. Device 2025;3:100752.
[34] Suh IS, Cho H, Lee M. Feasibility study on thermoelectric device to energy storage system of an electric vehicle. Energy 2014;76:436–44.
[35] Song W, Bai F, Chen M, Lin S, Feng Z, Li Y. Thermal management of standby battery for outdoor base station based on the semiconductor thermoelectric device and phase change materials. Appl Therm Eng 2018;137:203–17.
[36] Pakrouh R, Ranjbar AA, Hosseini MJ, Rahimi M. Thermal management analysis of new liquid cooling of a battery system based on phase change material and thermoelectric cooler. Appl Therm Eng 2023;231:120925.
[37] Ren R, Diao Y, Zhao Y, Liang L. Experimental study on top liquid-cooling thermal management system based on Z-shaped micro heat pipe array. Energy 2023;282:128321.
[38] Greco A, Cao D, Jiang X, Yang H. A theoretical and computational study of lithium-ion battery thermal management for electric vehicles using heat pipes. J Power Sources 2014;257:344–55.
[39] Chen K, Hou J, Song M, Wang S, Wu W, Zhang Y. Design of battery thermal management system based on phase change material and heat pipe. Appl Therm Eng 2021;188:116665.
[40] Hu Q, Luo D, Guo J, Qiu W, Wu X, Yang L, et al. Broad temperature Plateau for high thermoelectric properties of n-Type Bi2Te2.7Se0.3 by 3D printing-driven defect engineering. ACS Appl Mater Interfaces 2023;15:1296–304.
[41] Mali V, Saxena R, Kumar K, Kalam A, Tripathi B. Review on battery thermal management systems for energy-efficient electric vehicles. Renew Sustain Energy Rev 2021;151:111611.
[42] Hamisi CM, Gerutu GB, Greyson KA, Chombo PV. Thermal behavior of lithium-ion battery under variation of convective heat transfer coefficients, surrounding temperatures, and charging currents. J Loss Prev Process Ind 2022;80:104922.
[43] Luo D, Yang S, Zhang H, Cao J, Yan Y, Chen H. Performance improvement of an automotive thermoelectric generator by introducing a novel split fin structure. Appl Energy 2025;382:125218.
[44] Luo D, Yu Y, Yan Y, Chen W-H, Cao B. Increasing power densities in a thermoelectric generator by stacking and incorporating dual heat pipes. Device 2024;2:100435.
[45] Luo D, Wu H, Cao J, Yan Y, Yang X, Cao B. Numerical investigation of a battery thermal management system integrated with vapor chamber and thermoelectric refrigeration. J Clean Prod 2024;434:140089.
[46] Zhao D, Tan G. Experimental evaluation of a prototype thermoelectric system integrated with PCM (phase change material) for space cooling. Energy 2014;68:658–66.
[47] Ren R, Zhao Y, Diao Y, Liang L, Jing H. Active air cooling thermal management system based on U-shaped micro heat pipe array for lithium-ion battery. J Power Sources 2021;507:230314.
[48] Luo D, Wang R, Yu W, Zhou W. Parametric study of a thermoelectric module used for both power generation and cooling. Renew Energy 2020;154:542–52.
[49] Lindgren J, Lund PD. Effect of extreme temperatures on battery charging and performance of electric vehicles. J Power Sources 2016;328:37–45.
[50] Jiang ZY, Qu ZG. Lithium–ion battery thermal management using heat pipe and phase change material during discharge–charge cycle: a comprehensive numerical study. Appl Energy 2019;242:378–92.